Supplementary data

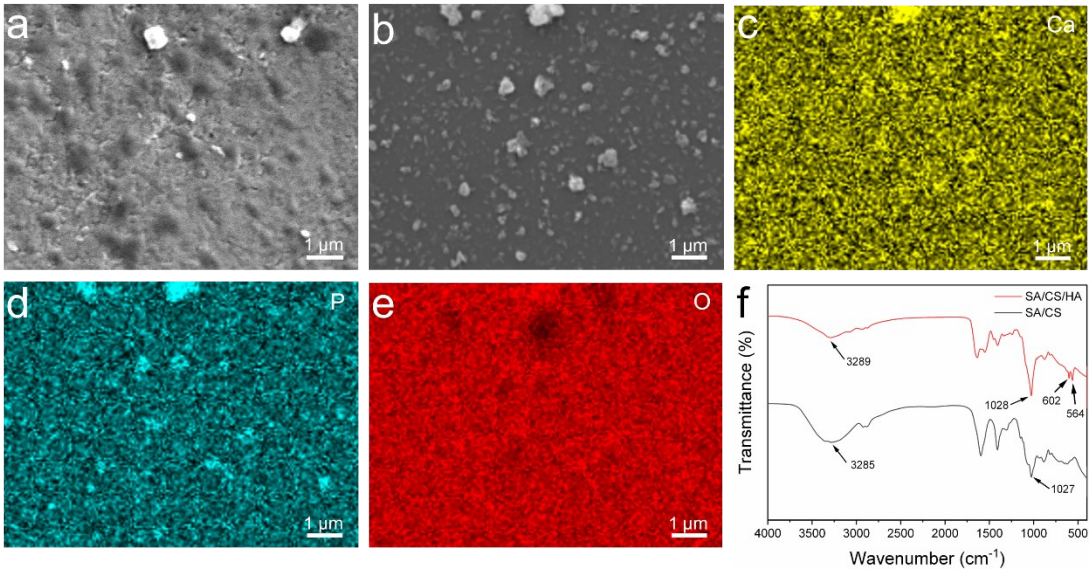

Figure S1. (a) SEM images of SA/CS layer. (b) SEM images of nanoHA seed layer. (c-e) EDS elemental mapping of nanoHA seed layer. (f) FT-IR spectra of the SA/CS layer and nanoHA seed layer.

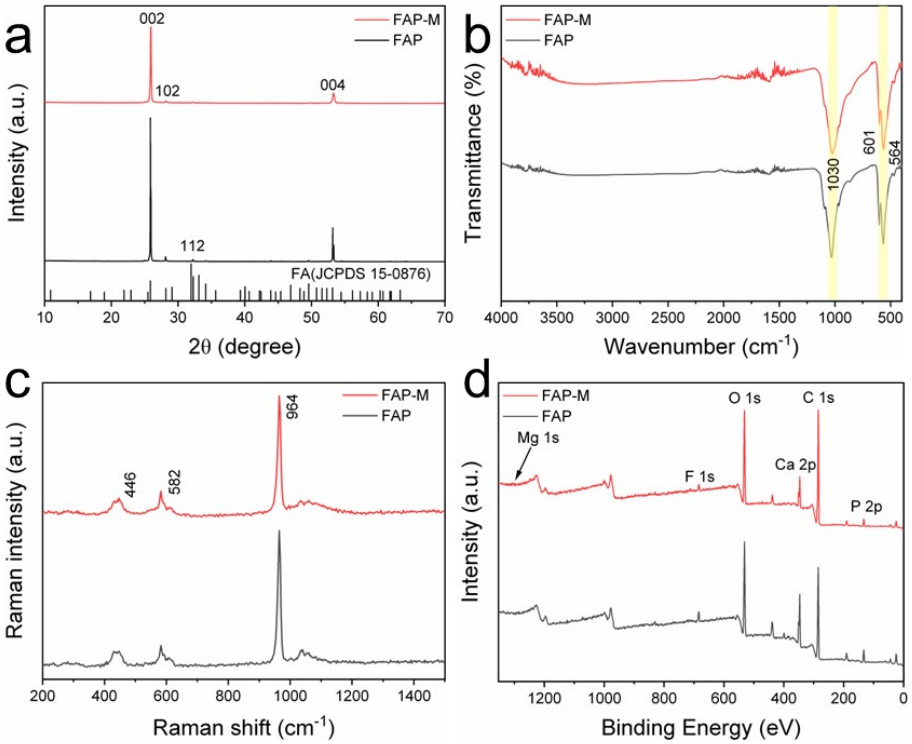

Figure S2. (a) XRD pattern of the FAP-M (controlled by 1.12 mM Mg^{2+}) and FAP (without Mg^{2+}) films. (b) FT-IR spectra of the FAP-M and FAP films. (c) Raman

spectra of the FAP-M and FAP films. (d) XPS survey spectrum of the FAP-M and FAP films.

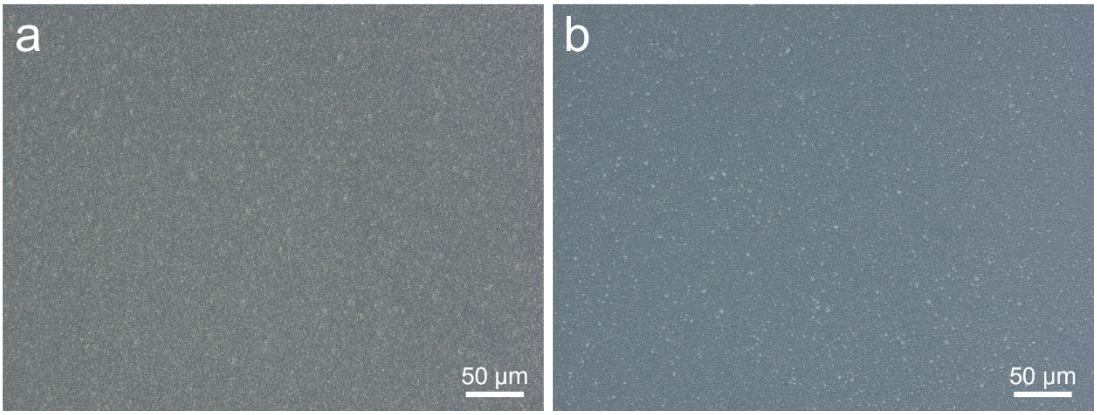

Figure S3. The Top-view ultra-depth-of-field micrographs of the (a) FAP (without Mg^{2+}) and (b) FAP-M (controlled by 1.12 mM Mg^{2+}) films.

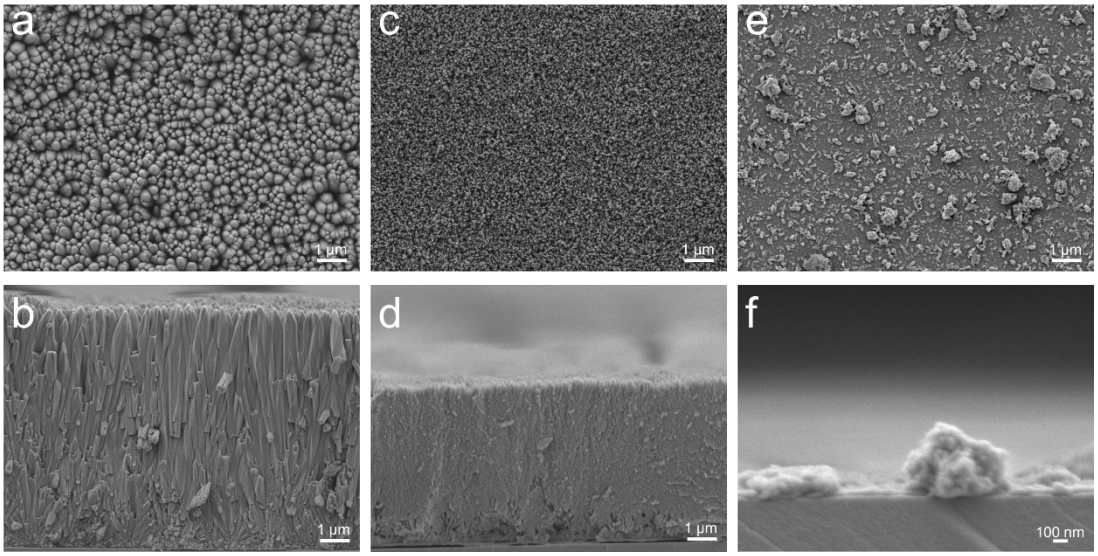

Figure S4. (a, b) SEM images of FAP-Mg films controlled by 0.56 mM Mg^{2+}. (c, d) SEM images of FAP-Mg films controlled by 2.24 mM Mg^{2+}. (e, f) SEM images of FAP-Mg films controlled by 4.48 mM Mg^{2+}.

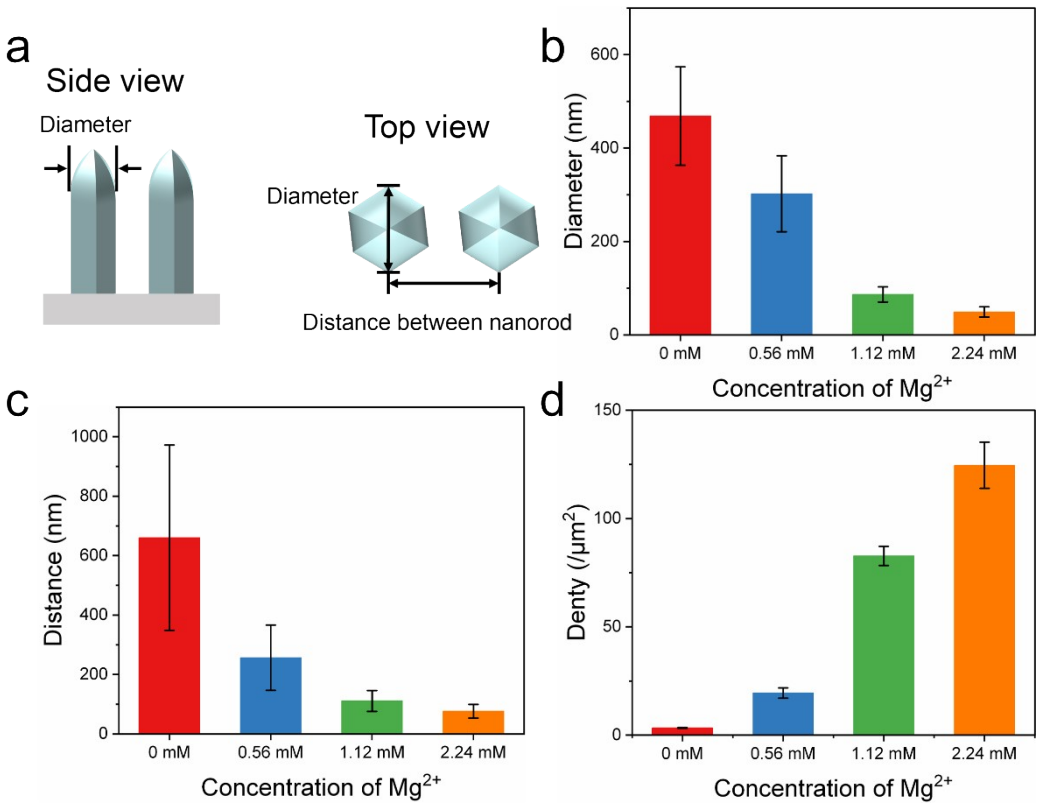

Figure S5. (a) Statistical analysis of the geometry of FAP nanorod. (b) Diameter, (c) Distance between nanorod, (d) The number density per area of the FAP arrays with different concentration of Mg^{2+}.

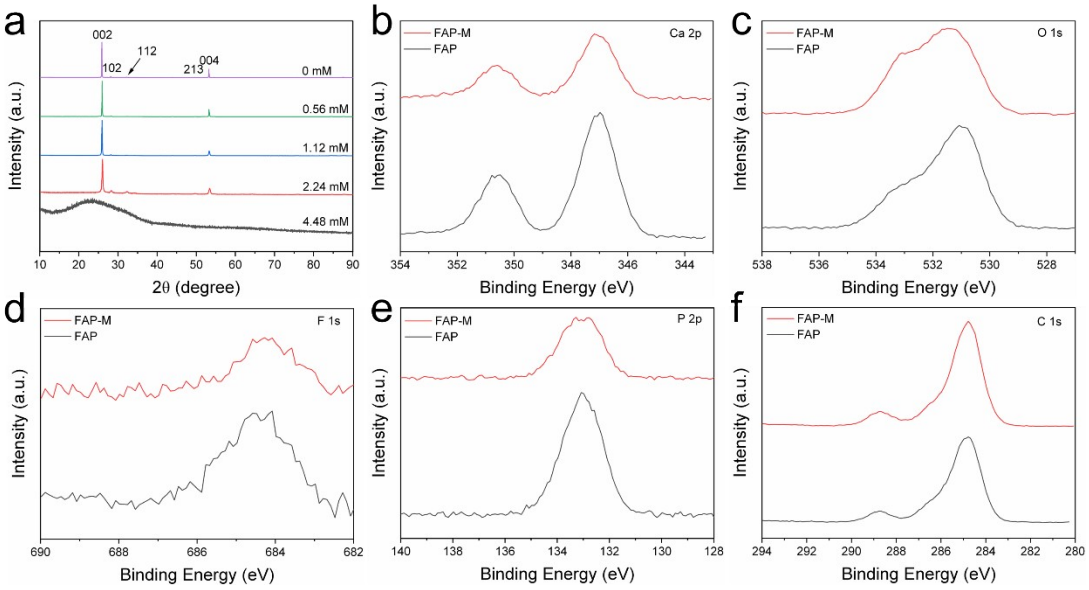

Figure S6. (a) XRD pattern of the FAP-M films with different concentration of Mg^{2+}. (b-f) High-resolution XPS profiles of the FAP-M (controlled by 1.12 mM Mg^{2+}) and

FAP (without Mg^{2+}) films: (b) Ca 2p, (c) O 1s, (d) F 1s, (e), P 2p, and (f) C 1s.

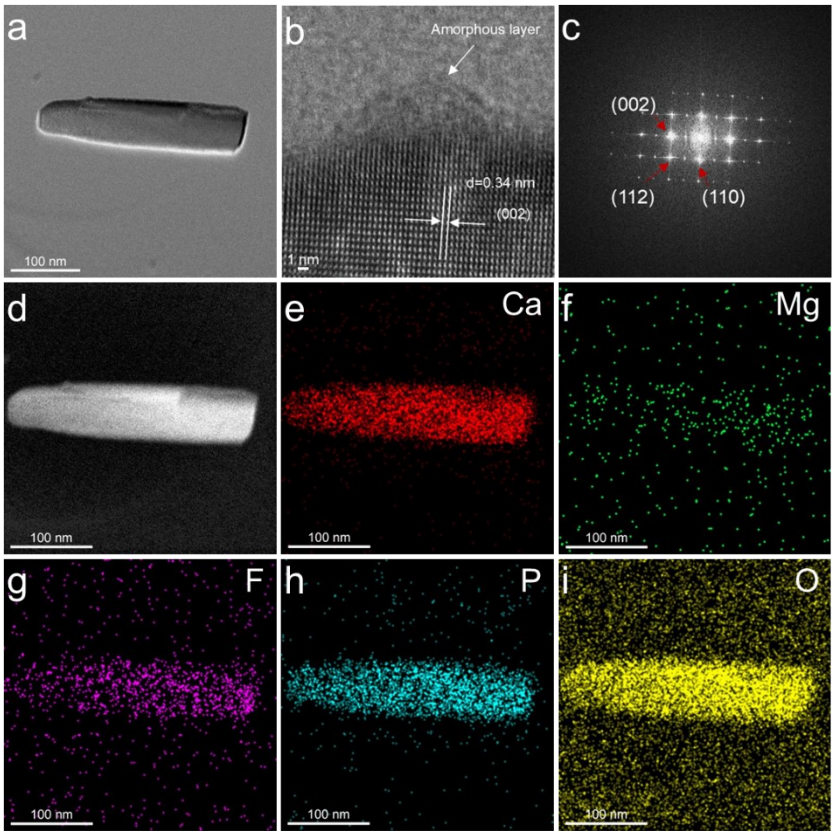

Figure S7. (a) TEM image of FAP-M nanorod controlled by 1.12 mM Mg^{2+}. (b) HRTEM image of FAP-M nanorod. (c) The FFT patterns of FAP-M nanorod. (d) TEM image in HAADF mode of FAP-M nanorod. (e-i) TEM-EDS mapping of FAP-M nanorod.

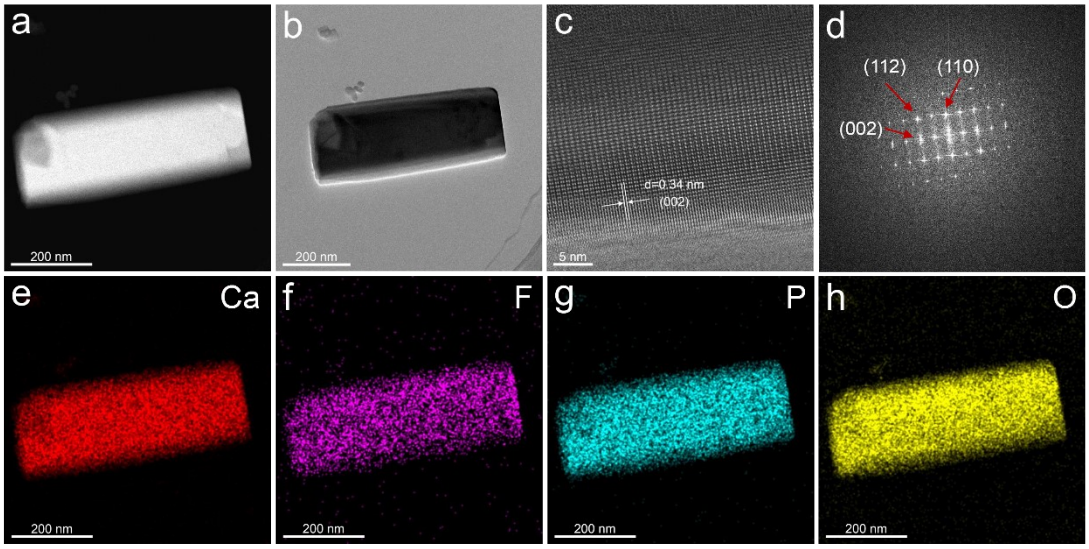

Figure S8. (a) TEM image in HAADF mode of FAP nanorod without Mg^{2+}. (b) TEM

image of FAP nanorod. (c) HRTEM image of FAP nanorod. (d) The FFT patterns of FAP nanorod. (e-h) TEM-EDS mapping of FAP nanorod.

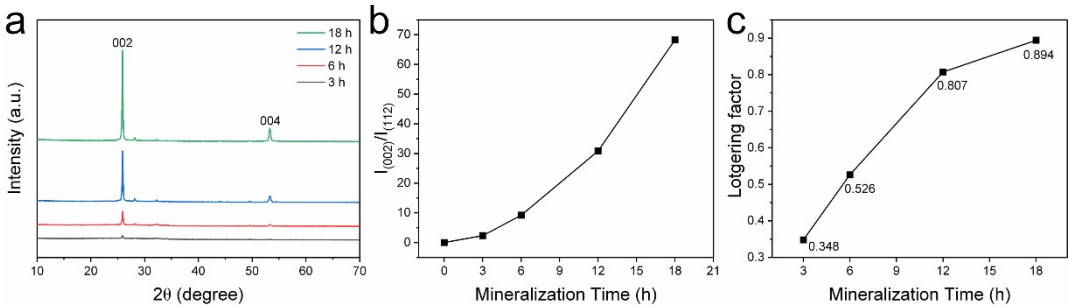

Figure S9. (a) XRD pattern during the reaction of the FAP-M films (3, 6, 12, and 18 h) controlled by 1.12 mM Mg^{2+}. (b) Intensity ratios of the (002) and (112) Bragg peaks of the FAP-M films during the reaction. (c) Lotgering orientation factor of the FAP-M films in different mineralization time.

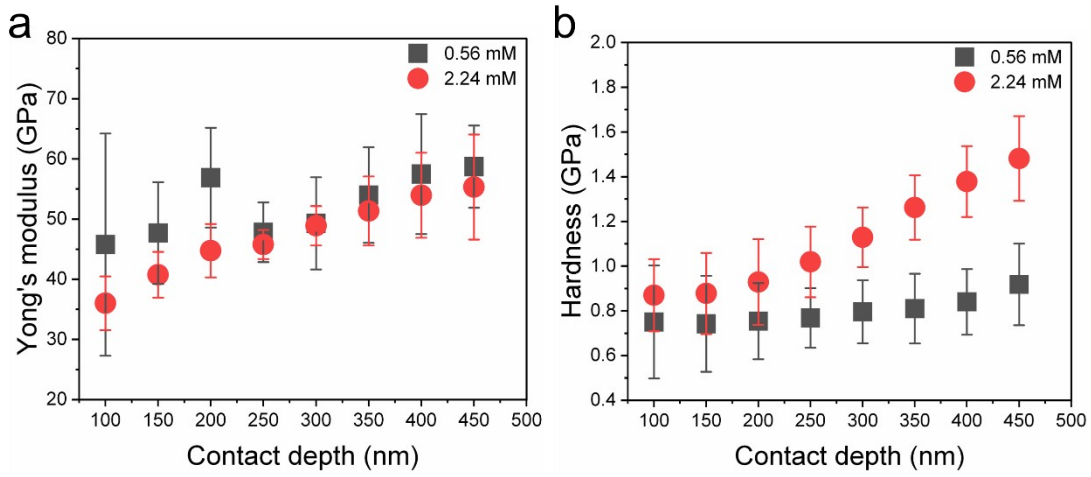

Figure S10. (a) Hardness−displacement curves and (b) Young's modulus-displacement curves of FAP-M films with 0.56 mM and 2.24 mM Mg^{2+}.

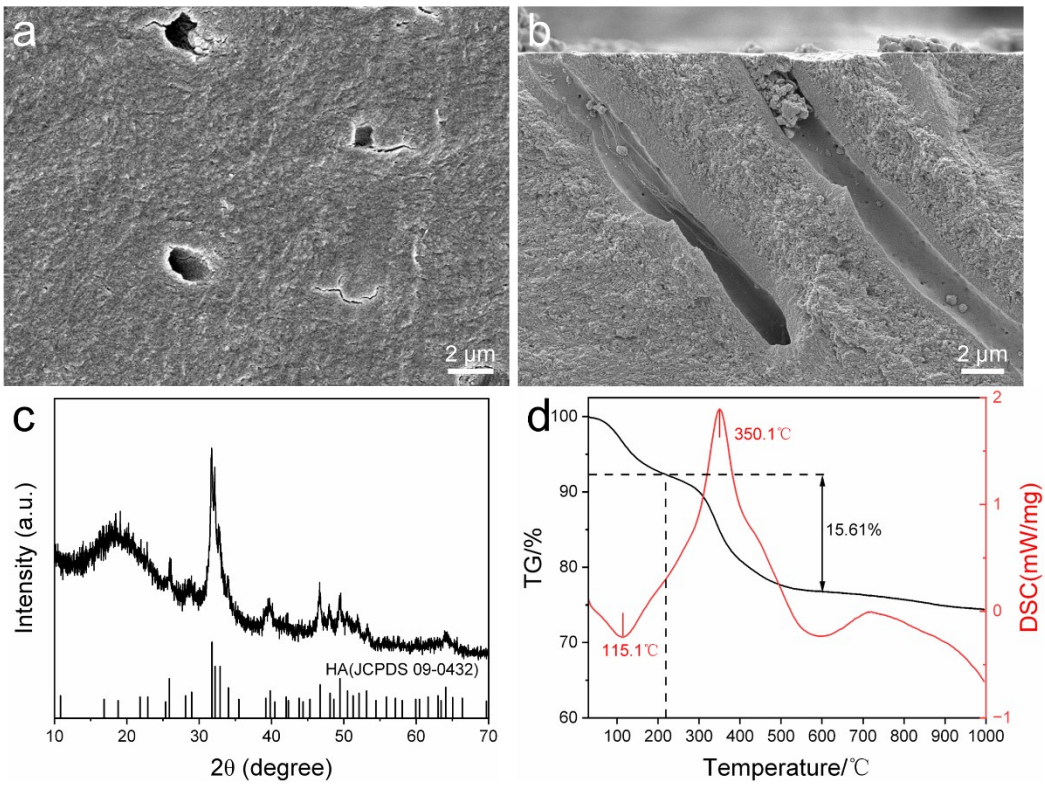

Figure S11. (a) The Top-view and (b) Cross-sectional SEM images of sound dentin. (c) XRD pattern and (d) TG-DSC curves of SD. SD: sound dentin.

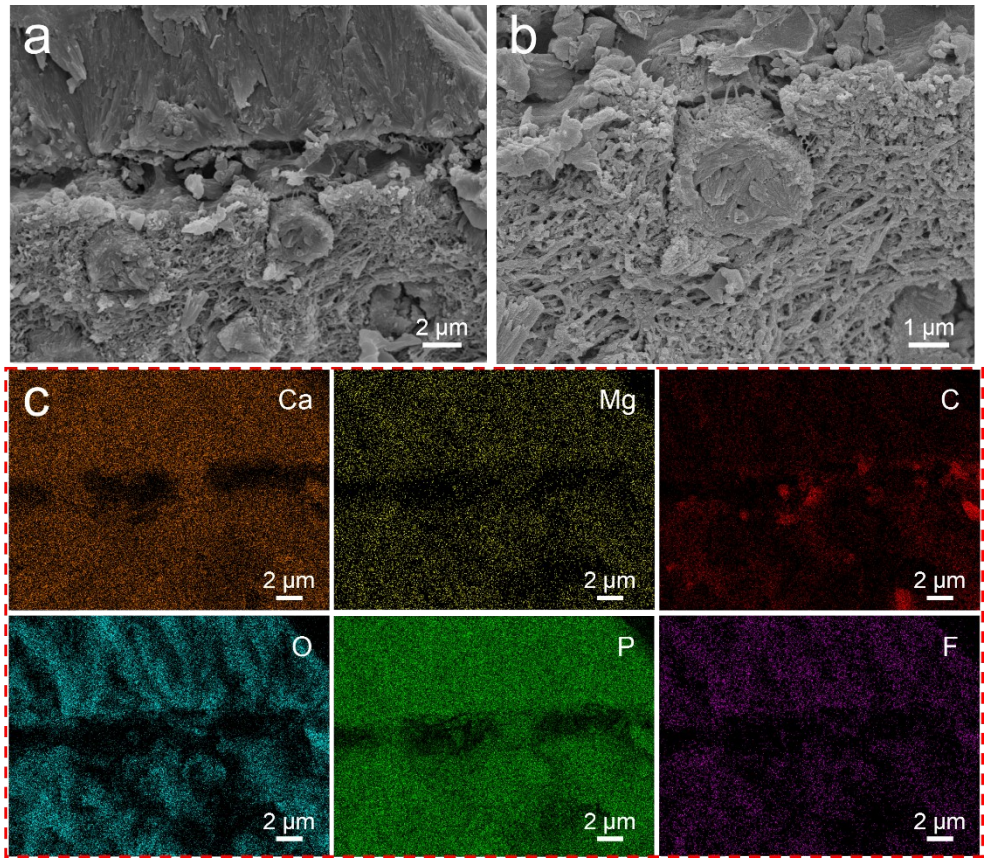

Figure S12. (a, b) The Cross-sectional SEM images of the FAP-M/dentin interface of

RD controlled by 1.12 mM Mg^{2+}. (c) EDS elemental mapping of the FAP-M/dentin interface.

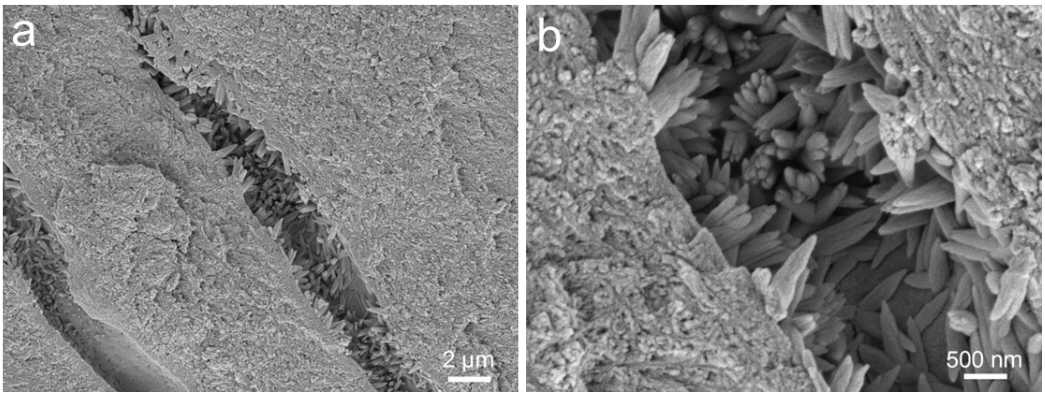

Figure S13. Cross-sectional SEM images of dentin tubules of remineralized dentin with FAP-M controlled by 1.12 mM Mg^{2+}.

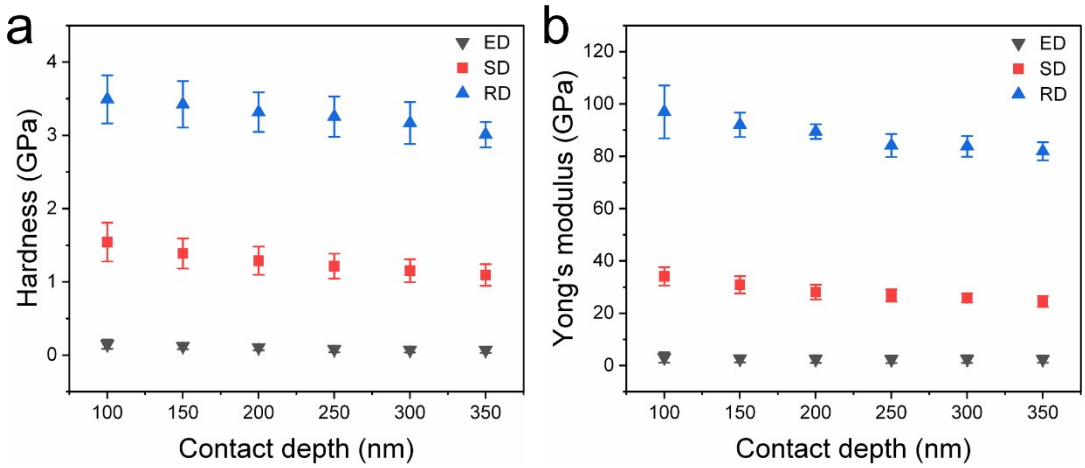

Figure S14. (a) Hardness−displacement curves and (b) Young's modulus−displacement curves of ED, SD, RD.